Deep-Sea Research II 100 (2014) 38–53

Contents lists available at ScienceDirect

Deep-Sea Research II

journal homepage: www.elsevier.com/locate/dsr2

Eddy properties in the Mozambique Channel: A comparison between observations and two numerical ocean circulation models

I. Halo [a,b,*], B. Backeberg [a,b,e], P. Penven [c], I. Ansorge [a], C. Reason [a], J.E. Ullgren [d]

[a] Department of Oceanography, University of Cape Town, Rondebosch 7701, South Africa
[b] Nansen-Tutu Centre for Marine Environmental Research, University of Cape Town, Rondebosch 7701, South Africa
[c] LMI ICEMASA, Laboratoire de Physique des Oceans (UMR 6523: CNRS, IRD, IFREMER), France
[d] NIOZ Royal Netherlands Institute for Sea Research, P.O. Box 59, 1790 AB Den Burg, Texel, The Netherlands
[e] Nansen Environmental and Remote Sencing Center, Thormøhlens gate 47, Bergen, Norway

ARTICLE INFO

Available online 6 November 2013

Keywords:
Cyclonic/anticyclonic eddies
Ocean models
Altimetry

ABSTRACT

Analysis of satellite altimetry observations, transports estimates from a mooring array, as well as output from two different numerical ocean circulation models (ROMS and HYCOM), have been used to investigate the mesoscale eddy properties and transport variability in the Mozambique Channel. The power spectral density of model transports at 17°S indicates the models ability to represent the transport variability at mesoscale frequencies (range between 3 yr^{-1} and 10 yr^{-1}). The models have shown an exaggerated representation of the lower frequencies ($\sim$ <3 yr^{-1}), while underestimating the higher frequency signals ($\sim$ >10 yr^{-1}). The overestimation of the seasonal cycle appears in our case not to be related to a misrepresentation of the mesoscale variability. The eddies were identified using an automatic eddy tracking scheme. Both anticyclonic and cyclonic eddies appeared to have a preferred site of formation within the channel. The density distribution showed that the anticyclones exhibited a bi-modal distribution: the first mode was associated with the typical scale for the oceanic mesoscale turbulence, while the second mode was related to the passage of large rings at a frequency of about 4–7 per year. On the other hand, cyclonic eddies had a single mode distribution that follows the first baroclinic Rossby radius of deformation, which is a typical scale for the oceanic mesoscale surface eddy variability, suggesting that their formation is associated with baroclinic instability. Eddy mean amplitudes per class of radius (<100 km), increase linearly with increasing radius, while no linear relationship exists for the rings. Different from the rings, the increase in the amplitude of the eddies was consistent with the increase of their life expectancy and travelling distances.

1. Introduction

The Mozambique Channel forms part of the greater Agulhas Current system, which extends from north of Madagascar to the southwestern extremity of South Africa (Lutjeharms, 2006). The greater Agulhas Current system is an important link in the exchange of heat and salt between the Indian and the Atlantic Oceans (Gordon, 1986; Weijer et al., 1999). It has been shown that the flux of warm and salty waters into the Atlantic Ocean via the Agulhas retroflection region plays a decisive role in maintaining the stability of the global meridional overturning oceanic circulation (de Ruijter et al., 1999), and hence the global climate (Beal et al., 2011).

An important way in which warm and salty waters from the Agulhas are transported into the South Atlantic is through the shedding of Agulhas Rings from the Agulhas retroflection south of Africa Lutjeharms and van Ballegooyen (1988); Reason et al., 2003). This mechanism has been termed the Agulhas leakage, and studies have shown that the frequency of Agulhas Ring shedding and thus the inter-ocean leakage is modulated by mesoscale perturbations originating upstream of the retroflection area, in the Mozambique Channel and South of Madagascar (Schouten et al., 2002; Penven et al., 2006; Biastoch et al., 2008b).

The flow through the Mozambique Channel is characterised by intense mesoscale eddy activity (Fig. 1), dominated by large anticyclonic eddies (Biastoch and Krauss, 1999; Ridderinkhof and de Ruijter, 2003; Schouten et al., 2003). These eddies play a significant role in the dynamics of the local marine ecosystems (Weimerskirch et al., 2004). It has been observed that these eddies trap anomalous water masses with higher nutrient and lower oxygen (Swart et al., 2010), and also advect coastal waters with high phytoplankton biomass into the offshore oceanic environment (Quartly and Srokosz, 2004; Omta et al., 2009; Tew-Kai and Marsac, 2009).

Mozambique Channel eddy characteristics have been determined from a number of measurements (Ridderinkhof et al., 2001; de Ruijter et al., 2002). Observations from a current metre mooring

* Corresponding author at: Department of Oceanography, University of Cape Town, Rondebosch 7701, South Africa.
E-mail address: issufo.halo@uct.ac.za (I. Halo).

0967-0645/$ - see front matter © 2013 Elsevier Ltd. All rights reserved.
http://dx.doi.org/10.1016/j.dsr2.2013.10.015

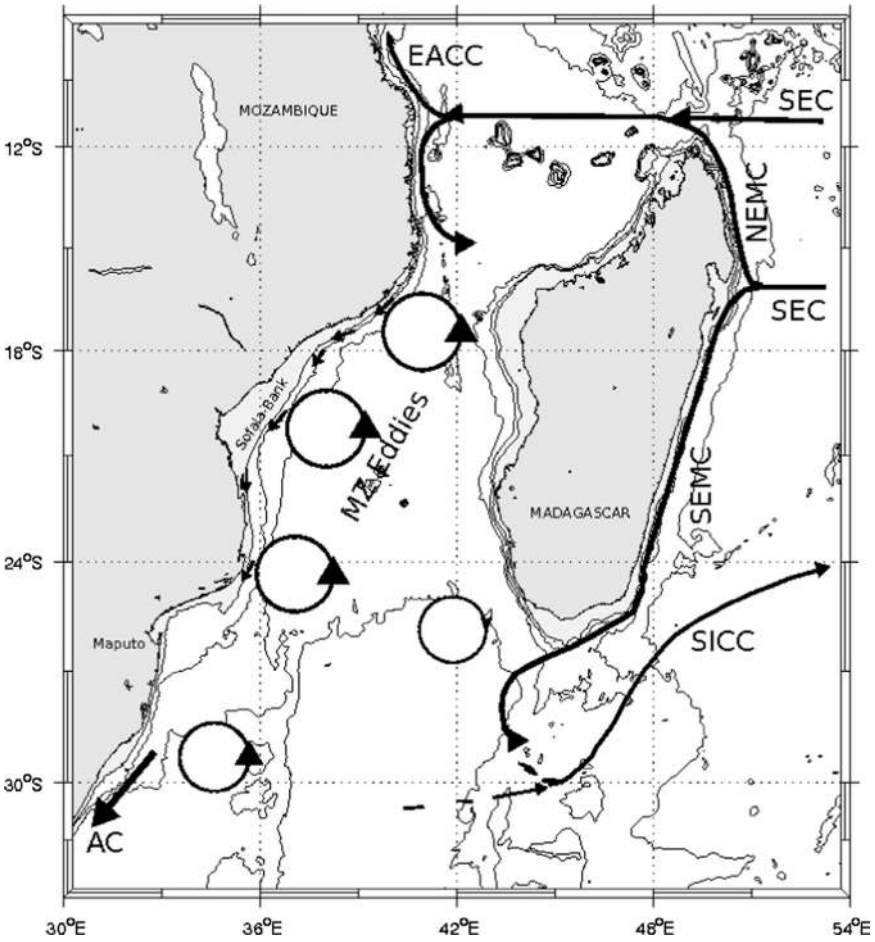

Fig. 1. Main oceanographic features of the circulation system in the Mozambique Channel, and region around Madagascar. South Equatorial Current (SEC), North East Madagascar Current (NEMC), South East Madagascar Current (SEMC), East African Coastal Current (EACC), South Indian Countercurrent (SICC), the Agulhas Current (AC) and Mozambique Channel eddies (MZ-Eddies). The arrows indicate the direction of the flow. The cyclic features represent the eddy field, being clockwise for cyclonic eddies and anticlockwise for anticyclonic eddies. The background contours show the isobaths at 200, 1000, 2000 and 4000 m. The grey shaded bathymetry is shallower than 200 m.

array at ~17°S (Ridderinkhof and de Ruijter, 2003) have shown that these eddies are up to ~300 to 350 km wide, can reach all the way to the bottom of the Channel (over 2000 m deep), and have a strong barotropic component (de Ruijter et al., 2002; Ridderinkhof and de Ruijter, 2003; Schouten et al., 2003).

These eddies have been shown to be surface intensified, propagating southward, parallel to the western boundary of the Channel, with speeds of ~6 km d^{-1}. Interestingly, between 18° and 21°S, their propagation speed reduces to 3–4 km d^{-1} (Schouten et al., 2003), but further to the south, at 24°S, analysis of the eddy properties by Swart et al. (2010), revealed that the eddy propagation velocities increase to > 6 km d^{-1}, with tangential velocities of about 0.5 m s^{-1}, while maintaining their large diameters (over ~200 km). On average, these eddies transport heat and salt of about 1.3×10 J and 6.9×10 kg, considered to be sufficient to modify the water masses downstream (Swart et al., 2010).

The frequency of occurrence of eddies is quite regular, observed to be about 4–5 per annum at 17°S (Schouten et al., 2003). Their passage induces fluctuations in the volume transport, ranging from approximately 20 Sv northward to 60 Sv southward. The mean poleward transport has been estimated to be 15 Sv (de Ruijter et al., 2002). However, this quantity seems highly variable: a lower transport of 8.6 Sv was found by Harlander et al. (2009), for the period 2003–2006, but using a longer time series, from the end of 2003 to early 2008, Ridderinkhof et al. (2010) estimated a transport of 16.7 Sv.

Due to the overwhelming signature of the anticyclonic eddies in the central Mozambique Channel, there is no conclusive evidence in the literature regarding the origin of cyclonic eddies in this region. Both cyclonic and anticyclonic eddies are important dynamical features for marine ecosystems (Robinson, 1983; Lathuiliere et al., 2011). They usually bring deep nutrient-rich waters into the upper ocean, thereby enhancing primary production. Currently, the role of the Mozambique Channel eddies in the local ecosystem is being investigated by hydrographic surveys, carried out as part of the MESOBIO programme (Ternon et al., 2013). However, despite their important role, little is known about their abundance and characteristics. For example, de Ruijter et al. (2002) found no cyclonic eddies in the Channel. The apparent cyclonic anomalies observed from altimetry in their study were attributed to artifacts in the data processing, and an inaccurate knowledge of the mean dynamic topography. They concluded that the cyclonic features are misrepresented simply because of the absence of anticyclonic eddies (de Ruijter et al., 2002). Thus, the present knowledge states: *"the frequent passage of positive anomalies through the Mozambique Channel leaves a signal in the mean SSH field, leading to a negative anomaly when no anticyclone is present"* (Schouten et al., 2003). Previous studies have identified cyclonic eddies in the Mozambique Channel Gründlingh (1995). However, their generation site was uncertain, and later studies (Schouten et al., 2003; de Ruijter et al., 2004) have suggested that these transitory features were generated at the southwestern edge of Madagascar, and not within the channel.

The present generation of state-of-the-art numerical ocean models have been shown to simulate the eddy regime in the Mozambique Channel with a reasonable degree of accuracy (Penven et al., 2006; Biastoch et al., 2008a; Backeberg et al., 2009). An extensive comparison of observed and modelled transport, seasonal cycle, and eddy frequencies in the narrows of the channel, has been conducted by van der Werf et al. (2010). This study suggested that the models in general overestimated the seasonal cycle because the spectral density at other frequencies is underrepresented. Van der Werf et al. (2010) used output from six ocean general circulation models, based on similar general characteristics, namely global ocean models using z-coordinate discretisation schemes.

Ocean models are usually classified according to their vertical discretisation (Song and Haidvogel, 1994; Bleck, 2002; Chassignet et al., 2006). In this study, the output from two regional models with very different vertical discretisation schemes, and horizontal grid resolutions, were compared against available observations. The two models were the Regional Ocean Modelling System (ROMS, Shchepetkin and McWilliams, 2005) and the Hybrid Coordinate Ocean Model (HYCOM, Bleck, 2002). ROMS and HYCOM are typical representatives of two alternatives of the z-coordinate models. These two models are at the forefront of new developments in ocean modelling, using alternative vertical discretizations, to achieve a more realistic representation of the ocean dynamics.

The regional models were specifically designed to accurately simulate the dynamics of the greater Agulhas Current system (details of these models are provided in section 2.1). The simulated eddies in the Mozambique Channel were compared with eddies observed from satellite altimetry using an eddy detection method to track eddies and monitor their evolution as they propagate southward through the Channel. Furthermore, the model-altimetry comparison was augmented by an evaluation of the model transport against observed transport through the narrows of the Channel near 17°S in a similar manner to van der Werf et al. (2010).

2. Methods

2.1. Model description

2.1.1. Regional ocean modelling system

The Regional Ocean Modelling System (ROMS) is a primitive equation model designed to realistically resolve basin-scale, regional and coastal ocean processes, at higher resolution (Shchepetkin and McWilliams, 2005). The model has a free surface and uses a topography-following σ vertical grid. The higher order numerical schemes of the model allow for an improved simulation of oceanic mesoscale processes. The subgrid-scale vertical mixing is parameterized by the K-profile (KPP) scheme of Large et al. (1994). The model uses a centred fourth-order horizontal tracer advection scheme for potential temperature and salinity, with a biharmonic diffusion operator rotated to follow the isopotentials (Marchesiello et al., 2009). This feature minimises the problem of spurious diapycnal diffusion which could arise in σ-coordinate models. At the open boundaries, the model uses an adaptive, mixed passive-active implicit radiation scheme that connects the model solution to the surrounding oceanic environment (Marchesiello et al., 2001) A detailed description of the model is given by Shchepetkin and McWilliams (2005).

2.1.2. The southwest Indian ocean model (SWIM) configuration

The ROMS based configuration (SWIM) encompasses the southwest Indian Ocean. The configuration was built using the ROMSTOOLS package (Penven et al., 2008) and has been specifically designed to simulate the dynamics of the Mozambique Channel. The domain extends from 0° to 77.5°E, and from 3° to 47.5°S, with a horizontal grid of 1/5° (~21 km at the mean latitude of the Channel). Considering that the first baroclinic Rossby radius of deformation in the Mozambique Channel ranges from 40 km in the south to 100 km in the north (Chelton et al., 1998), this resolution is sufficiently fine to resolve the mesoscale dynamics of the region. The model uses $N=45$ sigma layers in the vertical, with the controlling stretching parameters being $\Theta_s=5.5$ at the surface, and $\Theta_b=0$ at the bottom. For the transition between the layers, $hc=10$ (Haidvogel and Beckmann, 1999).

The model topography was interpolated to the SWIM grid from the GEBCO1 (Global Earth Bathymetric Chart of the Oceans) data. In order to preserve important bathymetric features, while limiting pressure gradient errors, the bathymetric smoothing factor was kept equal to $r=\nabla h/h$, where h is the depth of the bathymetry. At the surface, SWIM was forced with monthly climatology fluxes. The heat and fresh-water fluxes were derived from the COADS 1/2° resolution data (Da Silva et al., 1994). The wind stress used in the climatology experiment was derived from the QuickSCAT satellite scatterometer for the period 2000–2007, gridded at 1/2° resolution.

For the open lateral boundaries, we used a monthly climatology, gridded from the 1° World Ocean Atlas 2005 data (WOA2005, Conkright et al., 2002). The level of no motion for the calculation of the geostrophic currents at the boundaries was chosen to be 1000 m. A climatology experiment of the model was run for a 10 year period, and its outputs were averaged every 2 days. Integrated volume properties have shown that the model reached its dynamical equilibrium after a 3 year interval, therefore, we analysed SWIM outputs from year 4 to year 10. The ability of SWIM to accurately simulate the mesoscale variability in the southwest Indian Ocean has been demonstrated by Halo (2012).

2.1.3. Hybrid coordinate ocean model

The Hybrid Coordinate Ocean Model (HYCOM, Bleck, 2002) is a primitive equation model that combines the optimal features of isopycnic-coordinate and fixed-grid ocean circulation models in one framework, dynamically changing its vertical layer distribution between isopycnic (ρ) and Cartesian coordinates, adjusting to an optimal structure regularly. This adaptive (hybrid) vertical grid conveniently resolves regions of vertical density gradients, such as the thermocline and surface fronts.

A 1/10° resolution of HYCOM for the greater Agulhas Current system, with 30 vertical hybrid layers, was run in a 1-way nested configuration, where a coarser basin-scale HYCOM of the Indian and Southern Ocean (George et al., 2010) provides lateral boundary conditions for the regional model. For the slowly varying variables, the boundary condition calculations are based on the flow relaxation scheme (FRS, Davies, 1983) and the barotropic variables are treated in a hyperbolic wave equation for pressure and vertically integrated velocities (Browing and Kreiss, 1982, 1986), such that variability simulated in the outer model is transmitted to the regional model.

The geographical domain of the regional nested model of the greater Agulhas Current system extends from 0° to 60°E and from 10° to 50°S, which includes the Mozambique Channel. The nested model was initialised from a balanced field from the outer model, interpolated to the high resolution grid, and following a long spin-up period. Data from years 2001 to 2010 of the free-running hindcast simulation were used.

The model bathymetry was also derived from GEBCO1, which was interpolated to the model grid. Both the nested and outer HYCOM models were forced interannually, with six hourly

synoptic atmospheric forcing fields from ERA40 before 2002 and then using the operational analyses from the ECMWF. Cloud cover data from the Comprehensive Ocean-Atmosphere Data Set (COADS, Slutz et al., 1985) and precipitation data from Legates and Willmott (1990)were also applied. The ability of the nested model to realistically simulate the region has been documented by Backeberg et al. (2008, 2009). In particular the importance of a 4th order momentum advection scheme is highlighted, which greatly improved the dynamics of the model.

2.2. Data

2.2.1. Satellite altimetry data

Satellite altimeters provide information about variations in sea surface height, useful to study mesoscale ocean variability in regions where the internal deformation radius is higher than the resolution of the merged data. In regions where in situ observations are sparse, such as the Mozambique Channel, studies rely heavily on such altimeter observations. To date, altimetry data spans almost two decades, starting October 14, 1992.

The gridded data product produced by Ssalto/Duacs and distributed by AVISO, with support from CNES, combines altimeter measurements from a number of satellites through an interpolation mapping technique (Ducet et al., 2000). In this study, we used these gridded maps of absolute dynamic topography, that combine sea level anomaly observations merged from Jason-1, Envisat, GFO, ERS-1, ERS-2 and Topex/Poseidon with the Rio09 mean dynamic topography (Rio et al., 2011). The data are provided globally on a regular interpolated grid with a spatial resolution of $1/4^o \times 1/4^o$, every 7 days.

2.2.2. LOCO data

To evaluate the volume transport and its variability in the models, their outputs are compared with in situ observations from the Long-term Ocean Climate Observation program (LOCO, de Ruijter et al., 2006; Ridderinkhof et al., 2010). The LOCO mooring array is situated across the narrows of the Channel near 17°S, and each mooring includes current metres, temperature-conductivity-pressure sensors and Acoustic Doppler Current Profilers (de Ruijter et al., 2006; Harlander et al., 2009; van der Werf et al., 2010). This array has consistently measured mass and heat transport through the Mozambique Channel since 2003, following a pilot study in 2000–2001, thus representing the longest time series of in situ observations ever recorded in the Mozambique Channel. Details concerning the LOCO data, instruments and deployment strategy are given by Ridderinkhof et al. (2001), de Ruijter et al. (2002), Ridderinkhof and de Ruijter (2003), and Harlander et al. (2009). In the present study we used the data collected from 23 November 2003 to 16 December 2009, corresponding to four deployment periods, between which moorings were recovered, serviced and redeployed.

2.3. Eddy detection and tracking algorithm

Since the ocean circulation in the Mozambique Channel is dominated by the propagation of mesoscale eddies (de Ruijter et al., 2002), it is important that model simulations capture their properties adequately. In order to compare observed eddy properties to those simulated in the models in a robust and consistent manner, an eddy detection scheme was implemented.

Among the numerous algorithms employed, the two methods generally used with altimetry data are the methods based on geometric criteria, for example, detecting closed loops in SSH (Chelton et al., 2011), and the methods based on local deformation properties of the flow, mostly selecting regions where the Okubo-Weiss parameter is below a negative threshold (Isern-Fontanet et al., 2006; Chelton et al., 2007) (i.e. where the flow is dominated by vorticity). The Okubo-Weiss parameter is defined as $W=S_n^2+S_s^2-\xi^2$, where $S_n=\partial u/\partial x-\partial v/\partial y$, $S_s=\partial v/\partial x+\partial u/\partial y$, and $\xi=\partial v/\partial x-\partial u/\partial y$ (Okubo, 1970; Weiss, 1991), where u and v are the velocity components in the x and y directions.

In the case of altimetry, W is based on second derivatives of SSH. This amplifies the errors in measurements and interpolations, resulting in a significant level of noise (Chelton et al., 2011; Souza et al., 2011). A second problem is the sensitivity of the method in the choice of the threshold in W used for eddy detection (Chelton et al., 2011). Methods based on geometric criteria have appeared less problematic and have been shown to yield improved results compared to the Okubo-Weiss parameter (Chaigneau et al., 2008; Chelton et al., 2011; Souza et al., 2011). Nevertheless, they still require a threshold level to be set in for the SSH anomalies and/or criteria based on the shape of the detected structures (Chelton et al., 2011; Kurian et al., 2011).

To compare eddy statistics from different sources (altimetry and two ocean models), we need an algorithm independent of tunable parameters. By combining the Okubo-Weiss and geometric methods, the number of parameters is reduced. In this case, a geostrophic eddy is defined as contained within a close loop of SSH and dominated by vorticity ($W<0$). With a recently published improved mean dynamic topography (Rio et al., 2011) it is now possible to apply the eddy detection scheme to absolute SSH data rather than sea level anomalies. This has two major advantages in that (1) it prevents the spurious detection of current meanders, which are often associated with closed sea level anomaly loops, and (2) in a system dominated by large anticyclonic eddies, such as the Mozambique Channel, negative values of SSH anomalies are often interpreted simply as the absence of an anticyclonic eddy rather than the presence of a cyclonic eddy (de Ruijter et al., 2002). No specific treatment such as high pass filtering was applied to SSH.

An example of the application of the eddy detection scheme is given in Fig. 2 for 15 September 2003 (i.e. the date used by Weimerskirch et al., 2004). Initially the Okubo-Weiss parameter (W) was computed from the geostrophic velocities. Two passes of a Hanning filter were applied to reduce the grid scale noise. Regions dominated by vorticity were then represented by the grey contours in Fig. 2A. As discussed in Chelton et al. (2011), there is a high level of noise and several selected regions are obviously not mesoscale eddies. Next, regions inside a closed loop of SSH were selected. To prevent selecting an ocean gyre as a closed loop, a diameter limit of 600 km was set. Fig. 2B presents the features detected in the Mozambique Channel using this method. As noted by Chelton et al. (2011), in the case of altimetry, the geometric method appears to be more successful in detecting mesoscale geostrophic eddies. However, several problems still remained. Several structures with multiple cores were selected, for example at 17°S in the Mozambique Channel and at 24°S along the Mozambican coast, and elongated loops for example near 20°S west of the Madagascar West Coast.

By combining the regions of negative W (Fig. 2A) and the regions embedded in SSH closed loops (Fig. 2B), we obtained a more consistent pattern where the spuriously detected features associated with noise in W were excluded and the ambiguities in multi-poles/elongated closed loops were removed (Fig. 2C). Note for example the detection of a typical anticyclonic Mozambique Channel eddy between 16°S and 18°S in Fig. 2C and D in comparison with the pattern detected in Fig. 2A and B.

Three tunable parameters still remained: the interval between the contours for closed loop detection (2 cm), the maximum size of a closed loop (600 km), and the number of passes of the Hanning filter on W (2). Tests have shown that the number of detected eddies is not very sensitive to these parameters. They

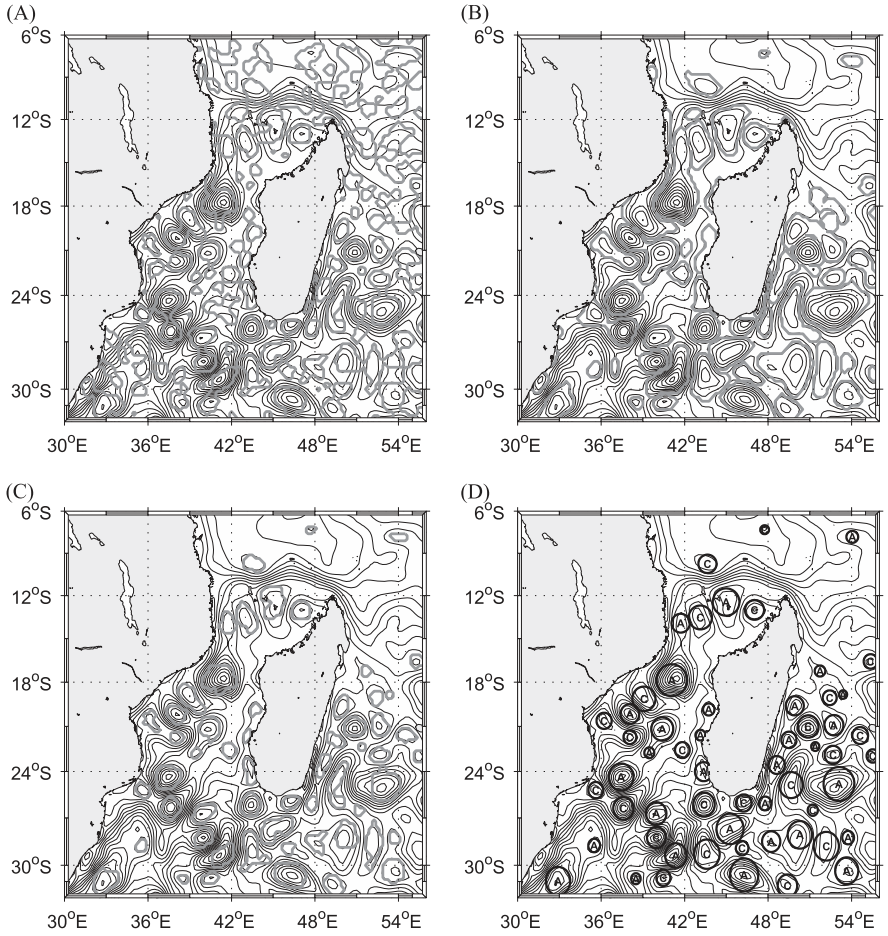

Fig. 2. Evaluation of the automatic eddy detection algorithm: (A) regions of negative Okubo-Weiss parameter, (B) regions enclosing a closed loop of SSH, (C) combination between Okubo-Weiss parameter and closed loop of SSH, (D) final result of the eddies identified and selected (A: anticyclones, C: cyclones). Black contours in the background correspond to the mean SSH. Data selected for 15 September 2003, as used by wei04, for comparison purposes.

were kept identical when detecting eddies from altimetry and the two different ocean models.

The algorithm used to track eddies in time follows the method proposed by Penven et al. (2005), where an eddy detected in one frame is the same eddy in the subsequent frame if a generalised distance in a non-dimensional property space is minimum:

$$X_{e1,e2} = \sqrt{((\Delta X/X_0)^2 + (\Delta R/R_0)^2 + (\Delta\xi/\xi_0)^2)} \quad (1)$$

where ΔX is the spatial distance between the eddy centres e_1 and e_2, ΔR is the variation of diameter, $\Delta\xi$ is the variation of vorticity, X_0 is a characteristic length scale (25 km), R_0 is a characteristic radius (200 km), and ξ_0 is a characteristic vorticity (10^{-5} s^{-1}). $X_{e1,e2}$ is considered infinite if there is a change of sign in vorticity to ensure that no cyclone becomes an anticyclone (i.e., the eddy should preserve its polarity). This eddy detection method is coded in MatLab and is freely available at http://www.simocean.org.za/tooleddy.php. Only eddies with a life-time greater than 30 days were considered in the present study.

3. Results

3.1. Transport at 17°S

The left panels in Fig. 3 show the total meridional transport across the narrows of the channel at 17°S for (a) LOCO, (b) SWIM and (c) HYCOM. The location of the section from which data for the models was extracted is shown in Fig. 4A. The right panels in Fig. 3 show the corresponding power density spectrum, based on a Multitaper Spectral Analysis. The spectrum is presented on a logarithmic scale to highlight a wider range of variability, especially the higher frequencies.

The observed mean poleward transport from LOCO was 16.3 Sv, while the simulated mean transports from SWIM and HYCOM were 18.6 Sv and 24.3 Sv respectively (1 Sv$=10^6$ m^3 s^{-1}). Maximum variations of the transport range from approximately 60 Sv southward to 40 Sv northward for LOCO. For SWIM the transport variations ranged from 60 Sv southward to 25 Sv northward, while for HYCOM transports were predominantly southwards with variations ranging from 3 Sv to 45 Sv.

The mean transport in SWIM was comparable in magnitude to the observations from LOCO, while HYCOM overestimated the mean transport by about 50%. Nevertheless, HYCOM was able to reproduce the interannual variability, in particular the increased poleward transport occurring from 2005 to 2007. High frequency transport fluctuations in LOCO showed strong levels of variability that overwhelm the seasonal cycle. These higher frequency signals were only partially represented in HYCOM, with a reduced strength (one order of magnitude) of the frequencies exceeding eight cycles per year. In SWIM, these high frequency signals were two orders of magnitude below the observed power density spectrum.

In the power density spectra (right panels of Fig. 3), the frequency range of variability can be separated into three bands of frequency: above 10 yr^{-1} (high frequencies), between 3 yr^{-1}

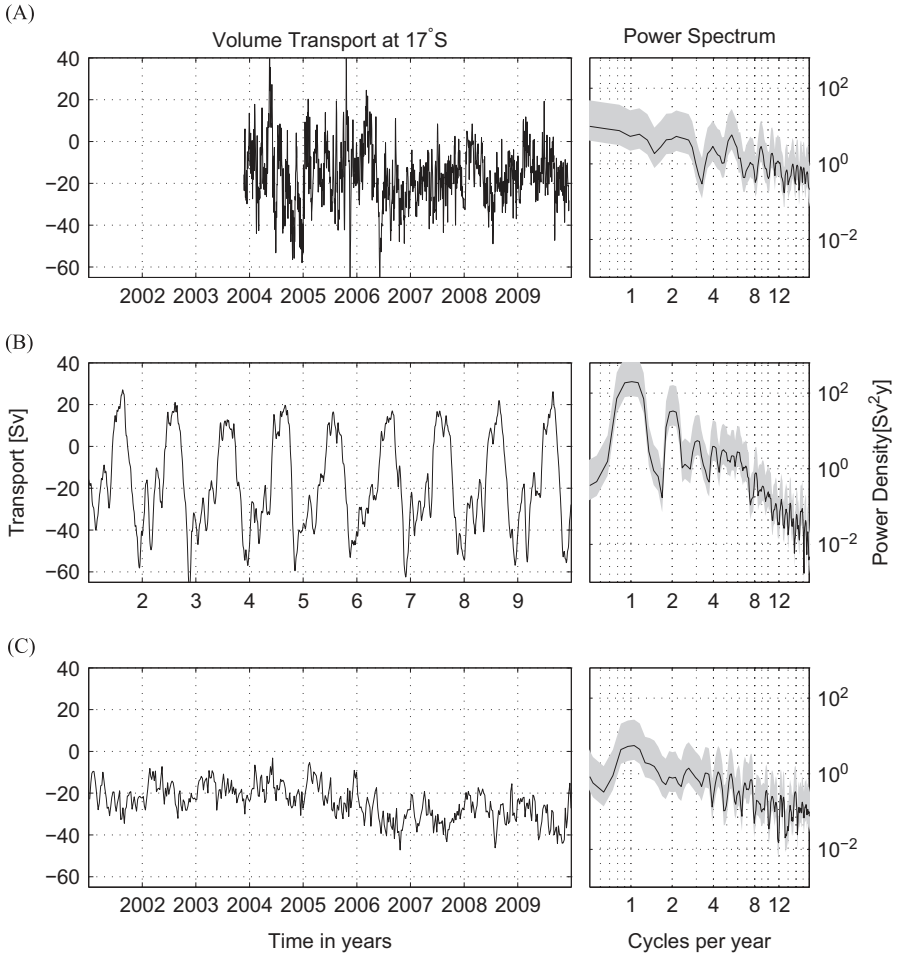

Fig. 3. Transport time series across the Channel narrows at 17 S, calculated with reference to the ocean bottom. Negative (positive) values indicate a southward (northward) transport: (A) LOCO, (B) SWIM and (C) HYCOM. The right panels show their corresponding power density spectra. The grey band indicates the 95% confidence level.

and 10 yr^{-1} (typical of the mesoscale regime), and below 3 yr^{-1} (the annual and semi-annual cycle, and interannual variations). Considering the model representations, it appears that the models overestimated the lower frequencies (i.e. the seasonal cycle), and underestimated the higher frequencies, with stronger exaggeration in SWIM than in HYCOM. In the mesoscale regime (i.e. range between 3 yr^{-1} and 10 yr^{-1}), the magnitude of the density spectra were in good agreement with the observations.

3.2. Variability of SSH

Fig. 4 shows the root mean square (RMS) of SSH, for altimetry from 14 October 1992 to 31 March 2010 (Fig. 4A), for SWIM for 7 years of climatology run (Fig. 4B), and for HYCOM from 2001 to 2010 (Fig. 4C). Enhanced levels of RMS SSH are representative of mesoscale variability. Both models were able to reproduce the enhanced mesoscale variability observed in the central Mozambique Channel, including the pattern that resulted from the southward propagation of these eddies travelling close to the Mozambican coastline (de Ruijter et al., 2002). HYCOM simulated maximum RMS magnitudes (~20 cm) occurring in the central Mozambique Channel, comparable to the observations from altimetry. Although the geographical extent of RMS exceeding 20 cm was limited to a smaller region, confined to the western part of the domain south of 20°S. SWIM overestimated the RMS by almost 50%. Furthermore, the spatial extent of these high levels of variability was broader, both to the north and in the centre of the Channel. In the southeastern region, the variability in both models is approximately 50% less than observed from altimetry.

3.3. Eddy vertical structure at 17°S

The vertical velocity structure across a Mozambique Channel anticyclonic eddy at 17°S, as described by de Ruijter et al. (2002), from SWIM and HYCOM is given in Fig. 5. These snapshots confirm that the eddies simulated in the models have similar vertical structures as those observed from in situ measurements (de Ruijter et al., (2002), see their Fig. 4B for comparison). The eddies are large, spanning almost the entire width of the narrow channel. They also reach the bottom of the channel, which is about 2500 m deep. This is consistent with observations (de Ruijter et al., 2002; Ridderinkhof and de Ruijter, 2003). SWIM simulated a maximum surface poleward flow of ~1.1 m s^{-1} at the western boundary of the section (Mozambique side), and an equatorward component at the eastern boundary (Madagascar side) which was relatively smaller (0.8 m s^{-1}). To the east of the eddy, a poleward surface flow was also evident over the Madagascar continental slope, with a maximum velocity of ~0.1 m s^{-1} centred near 500 m. This southward flow, also mentioned by Harlander et al. (2009), may be the precursor of an anticyclonic eddy forming in the centre of the Channel. HYCOM also reproduced comparable magnitudes, with a poleward component of ~1.2 m s^{-1} and an equatorward component of ~0.9 m s^{-1}. The poleward surface flow to the east of the eddy over the Madagascar continental slope was also evident, with a maximum velocity of ~0.5 m s^{-1}

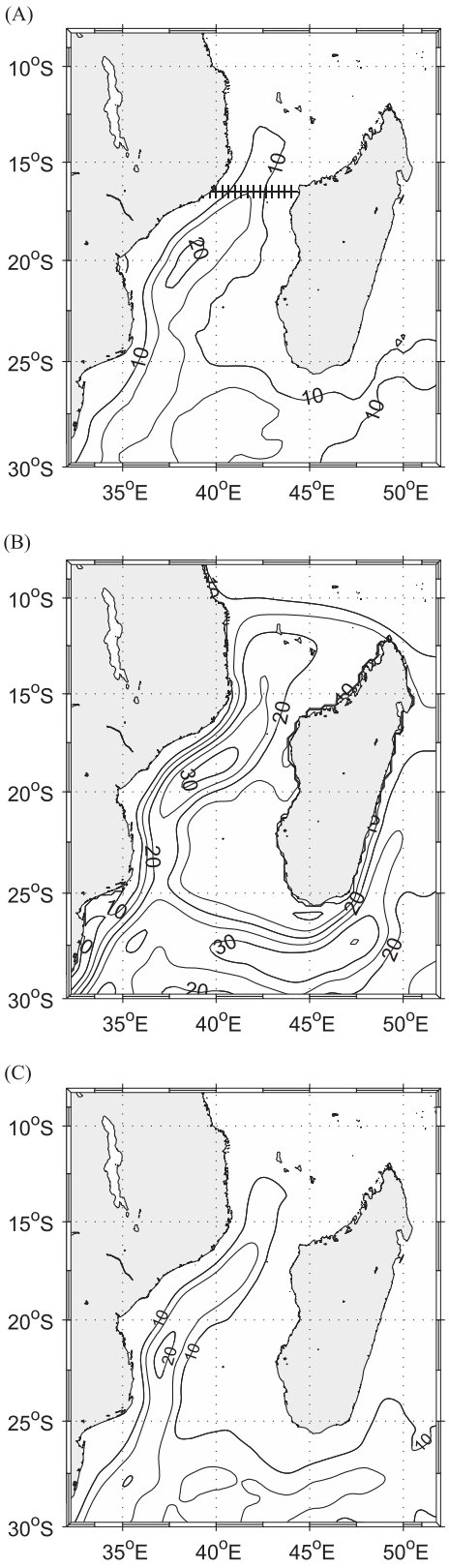

Fig. 4. Ocean variability expressed as root mean square of sea surface height (cm): (A) AVISO, (B) SWIM and (C) HYCOM.

centred near the surface (~100 m depth). The eddy in SWIM reached the Channel bottom with a maximum poleward component of 0.2 m s^{-1} and an equatorward component of ~0.1 m s^{-1}, while HYCOM reached the Channel bottom with a maximum poleward component of ~0.3 m s^{-1} and an equatorward component of ~0.1 m s^{-1}. The eddies appeared to be surface intensified and exhibited a strong barotropic component as also reported in observational studies (de Ruijter et al., 2002; Ridderinkhof and de Ruijter, 2003; Schouten et al., 2003). Interestingly, the HYCOM section was able to simulate the deep equatorward flow of the Mozambique Undercurrent, centred at an intermediate depth of ~1500 m, on the western side of the section over the Mozambican continental slope. This is also consistent with in situ observations (de Ruijter et al., 2002). On the other hand, SWIM simulated a relatively stronger poleward Undercurrent, with a maximum of 0.2 m s^{-1} at the eastern boundary of the Channel below 2000 m. In general, and in comparison to van der Werf et al. (2010), the vertical structure of the eddies seems to be well represented in the two regional models.

3.4. Eddy generation site and trajectories

Fig. 6 shows the positions and trajectories of eddies tracked in the Mozambique Channel over a 5 year period for eddies with a life time longer than 30 days. Only eddies between 32°–48.5°E and 24°–14°S were tracked. From this data it was possible to identify regions in the Mozambique Channel favoured by cyclonic or anticyclonic eddies, their formation and pathways. The eddy formation site is indicated by black circles, and their trajectories are represented by continuous lines. Large anticyclonic eddies (radius ≥100 km) are presented in red. A high concentration of circles can be considered as a primary site for eddy generation.

Anticyclonic eddies (left panels, Fig. 6), tended to form near 12°S to the west of Cape Amber, between Madagascar and Mozambique around the Comoros Archipelago. Interestingly, these data identify a secondary anticyclonic eddy formation region south of the narrows in the eastern boundary of the Channel near 20°S, 43°E. This secondary site was evident in the altimetry and both model simulations and has to date not been discussed in the literature.

Cyclonic eddies (right panels, Fig. 6) appear to be ubiquitous and their distribution in the channel is less defined. Nevertheless there was a tendency toward favouring the eastern part of the channel near the Madagascar coastline. A localised site for generation of cyclonic eddies appears to be at the northern entrance of the narrow channel, near 16°S, 44°E. At the western edge of the Channel near the Mozambique coast (Fig. 6) there was a localised site for the generation of cyclonic eddies near 17°S. In the south, at the eastern edge of the Channel, a site for cyclonic eddy formation was evident near 24°S, 44°E.

Anticyclonic eddies displayed a very regular southward propagation, predominantly tracking in the western part of the Channel closely following the Mozambique coastline. This was particularly true for the large anticyclones. On the other hand, cyclonic eddies appeared to propagate mostly in a southwestly direction.

Fig. 7 shows the frequency of occurrence for both cyclonic and anticyclonic eddies (in %), on a 1/2° × 1/2° grid for all the eddies tracked from 14 October 1992 to 31 March 2010. Higher frequencies were more evident for anticyclonic (left panels Fig. 7) than cyclonic eddies (right panels Fig. 7). For anticyclonic eddies, higher frequencies appeared also along the western boundary of the Channel, indicative of the eddies propagating southwestly along the main pathway. A secondary propagation pathway seems to begin in the eastern part of the channel, near 20°S, 44°E, and was more south-southwesterly, consistent with Fig. 6.

3.5. Eddy statistical census

Table 1 summarises the basic eddy properties (such as the number of eddies tracked per year, their mean lifetime, amplitude and diameter) from 14 October 1992 to 31 March 2010 for AVISO,

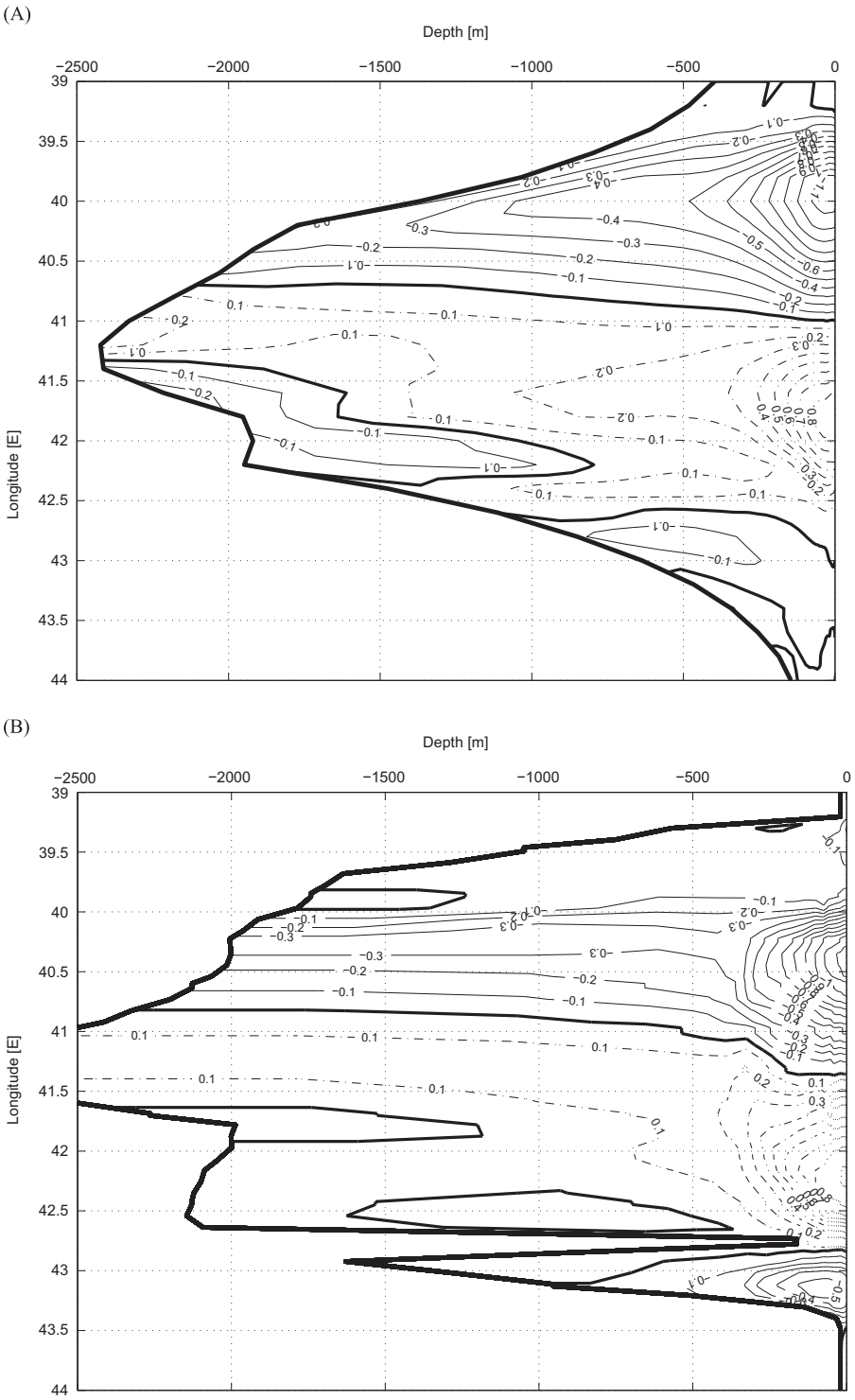

Fig. 5. Eddy vertical structure at 17°S: (A) SWIM, (B) HYCOM. See Fig. 4A for the section line. The thin continuous (discontinuous) isolines indicate poleward (equatorward) flow. The continuous bold contour indicate the isoline of 0 m s^{-1}. Within the 0 m s^{-1} bold contour the flow is equatorward in the western side of the channel and poleward in the eastern side. Note that the topography in SWIM is not accurately represented due to its relatively lower resolution.

a 7 year climatology run for SWIM and from 2001 to 2010 in HYCOM. From this data it is evident that there were more cyclonic than anticyclonic eddies in the Channel each year. Cyclonic eddies were in general smaller, with shorter life-spans, and had lower amplitudes than anticyclonic eddies. Overall, the modelled eddy properties were comparable with observations. The altimetry data indicated that a total of 39.2 cyclonic and anticyclonic eddies were tracked in the Channel each year, 56.4% of these were cyclonic, while 43.6% were anticyclonic.

In SWIM, an average total of 34.0 eddies were tracked each year, with 51.5% being cyclonic and 48.5% anticyclonic. The total number of anticyclonic eddies in SWIM was in good agreement with altimetry, while the number of cyclonic eddies was underestimated by 22.6%. Also, the anticyclonic eddies in SWIM were larger by ~17%. The SWIM anticyclones had 50% higher amplitudes than observed in altimetry. The 50% exaggeration in SSH RMS may be explained by this overestimate in anticyclonic eddy amplitude. The amplitudes and diameters of cyclonic eddies

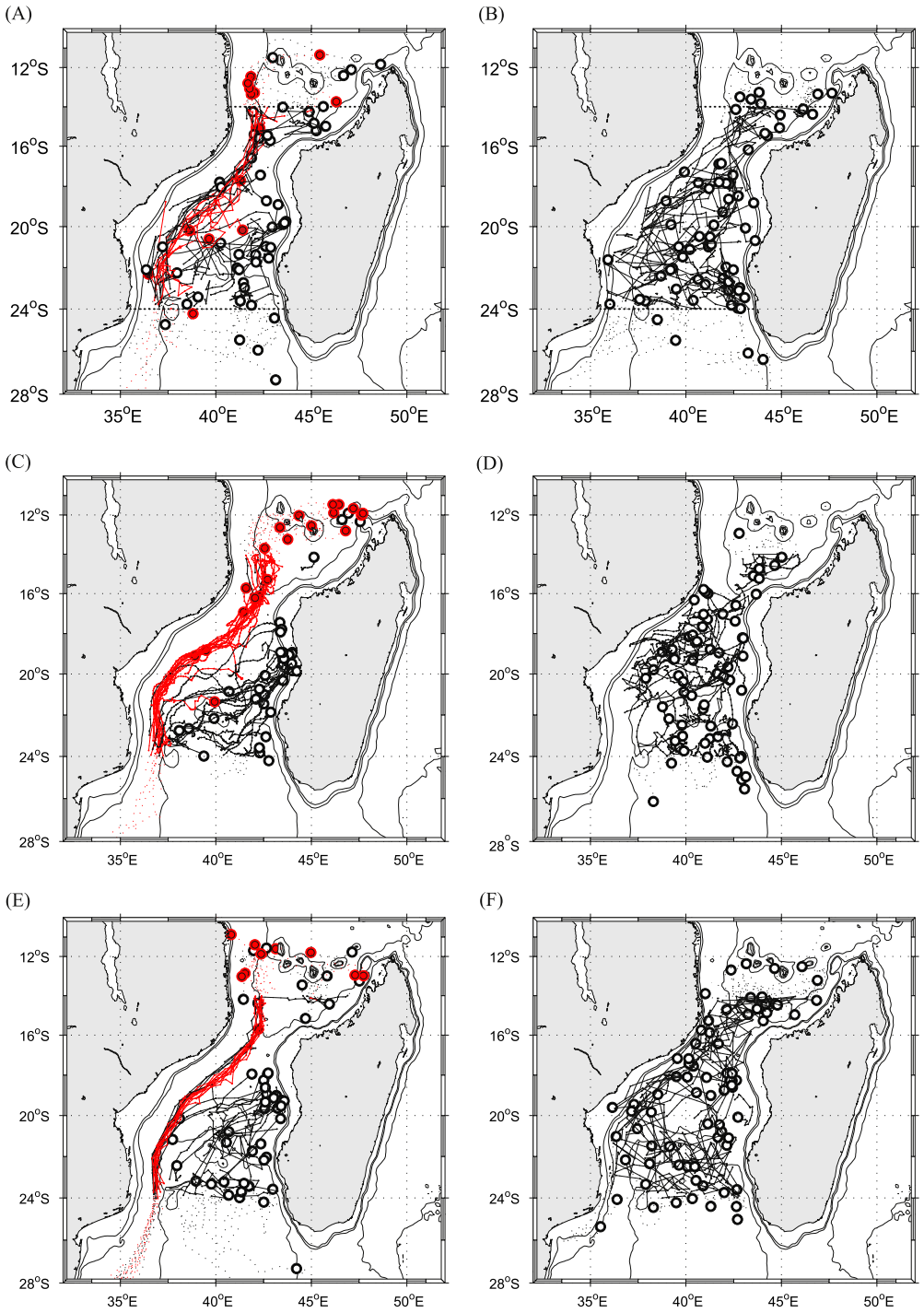

Fig. 6. Tracks of eddies for a 5 year period and their formation sites: (A,C,E) anticyclonic eddies (black) and rings (red), (B,D,F) cyclonic eddies. Solid black circles indicate the formation site, and the lines show their trajectories. Background contours are the isobaths at 500, 1000, 3000, 5000 m. The horizontal dashed lines at 14°S and 24°S (A, B) limit the area in which the study was made. (A, B)-AVISO, (C, D)-SWIM, (E, F)-HYCOM.

were reasonably well represented in SWIM, but their lifespan was underestimated by 37.6% compared to the altimetry observations.

In HYCOM, an annual mean total of 50.6 eddies was found, with 58.7% being cyclonic and 41.3% anticyclonic. The total number of cyclonic and anticyclonic eddies in HYCOM was relatively higher than the altimetry observations. The number of cyclonic eddies was overestimated by about 34.4% and the anticyclonic by about 22.2%. The eddies in HYCOM were generally smaller, with reasonably sized anticyclonic eddies, but the cyclonic eddies were underestimated by 23%. Similarly, the amplitude of the anticyclonic eddies in HYCOM was comparable to altimetry, but the amplitude of the cyclones was underestimated by 45%. The lifetime of the cyclonic eddies simulated in HYCOM was comparable to those observed from altimetry. However, the lifespan of anticyclonic eddies was overestimated by 22%.

Fig. 8 shows the frequency distribution of the eddy diameters, for altimetry, SWIM and HYCOM. The cyclonic eddies (Fig. 8, upper panels) observed by altimetry had a near symmetric distribution in terms of their radius, centred around 70 km. This is in agreement

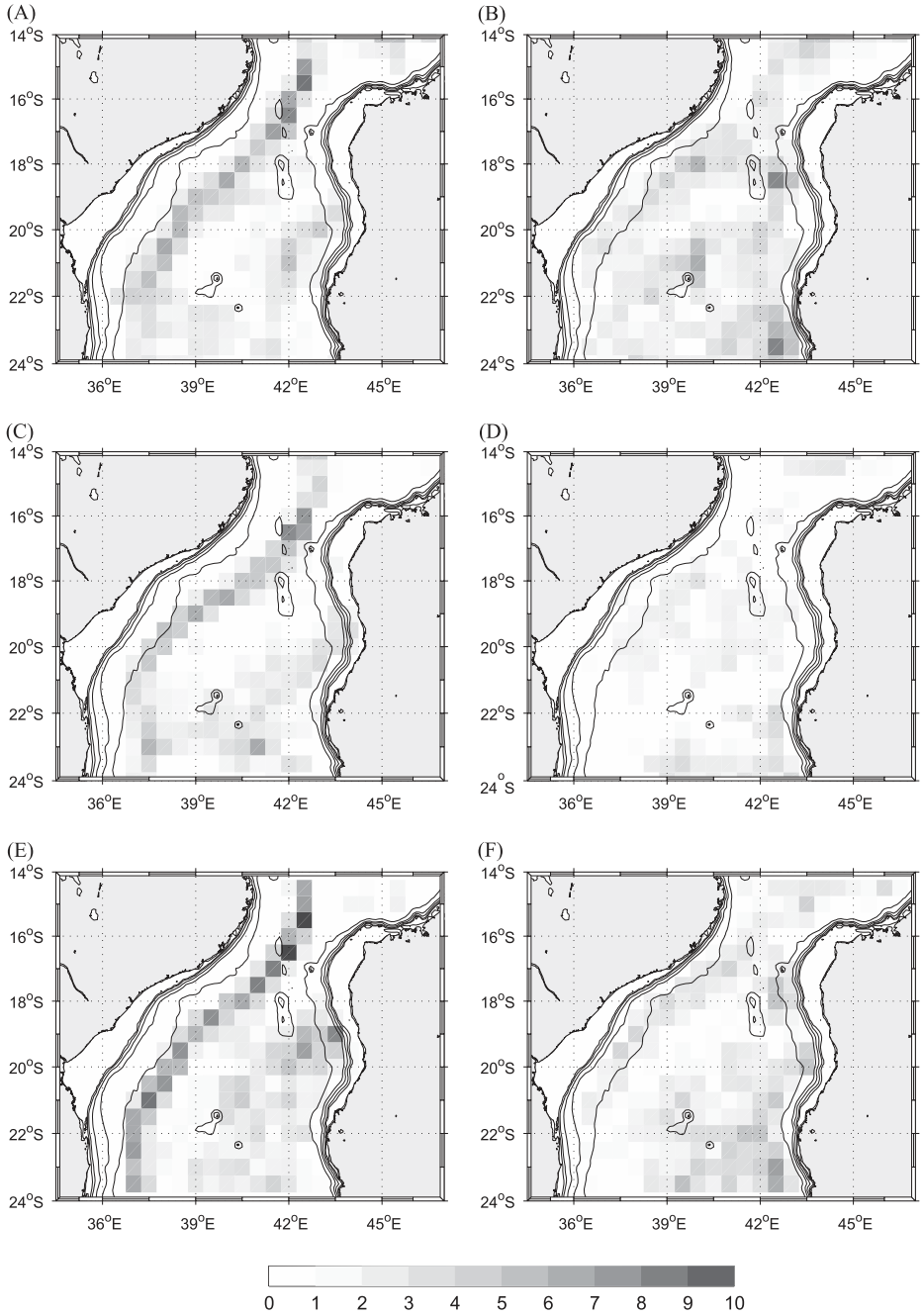

Fig. 7. Frequency of occurrence of all tracked eddies in % within an area of ½° × ½° grid size: (A, B) AVISO anticyclones and cyclones, (C, D) SWIM anticyclones and cyclones, (E, F) HYCOM anticyclones and cyclones.

with SWIM, while in HYCOM the highest peak was centred at 40 km radius. The peak at 70 km corresponds to the mean baroclinic Rossby radius of deformation in the Mozambique Channel (Chelton et al., 1998), which is consistent with the expected size of the mesoscale oceanic turbulence at this latitude.

In contrast to cyclonic eddies, anticyclones exhibited a bi-modal distribution, with observed diameters peaking at 60 km and 100 km for AVISO. In SWIM, the two peak diameters peaks were slightly larger at 70 km and 120 km, while in HYCOM they were in good agreement with the altimetry observations of 60 km and 100 km. The eddy radius of 100 km appears to be the cut off scale (Fig. 8), separating the larger from the smaller mode (i.e. first mode: eddy radius < 100 km; second mode: eddy radius ≥ 100 km).

The total number of anticyclones in each mode can be estimated by dividing their number by the total number of years that they were tracked. In the first mode, the following yearly averages were obtained: 12.7 for AVISO, 9.9 for SWIM, and 15.2 for HYCOM. The same calculation for the second mode yielded 4.4 for AVISO, 6.7 for SWIM and 5.7 for HYCOM. Note that the number of anticyclonic eddies per year in the second mode is in good agreement with the frequency of about 4–6 large anticyclonic eddies per year observed at the narrows of the Channel (Schouten et al., 2003; Harlander et al., 2009; van der Werf et al., 2010). Hence this second mode corresponds to the large Mozambique Channel anticyclones described in the literature (de Ruijter et al., 2002; Ridderinkhof and de Ruijter, 2003; Schouten et al., 2003).

The marked bimodal distribution in the radius of the anticyclones was an indication of the presence of two different types of anticyclonic coherent structures in the Mozambique Channel. To distinguish between these two types, a composite of sea surface

height, azimuthal velocity and vertical component of vorticity as a function of the distance from the centre of the eddies was derived from SWIM simulation, from year 4 to year 10 in the region 24°–14°S and 32°–47°E (Fig. 9). Only one model simulation is presented here for clarity. These properties were averaged for all the cyclones, anticyclones with a radius shorter than 100 km, and anticyclones with a radius larger than 100 km. The radial distances were addimentionnalized by the radius of each eddy. Inspection of Fig. 9 shows that the sea surface height roughly follows a typical "bell shape" pattern around the centre of each type of eddy (Fig. 9A), in agreement with (Chelton et al., 2011). While the amplitude and the slope were much larger for the large anticyclones, the small anticyclones and the cyclones presented a similar structure. The sharp slope in sea surface height coincided with a maximum in azimuthal velocity at the edge of the large anticyclones (Fig. 9B). This confirmed the ability of the eddy detection method for detecting eddy radii. The azimuthal velocities followed the piecewise model proposed by Castelão and Johns (2011) for the North Brazil Current rings: a quasi linear profile for $r < R_{eddy}$ and an exponential decay for $r > R_{eddy}$ (r being the radial distance to the eddy centre and R_{eddy} being the eddy radius). The smaller anticyclones and the cyclones followed a relatively flat Gaussian profile. This pattern was confirmed by vorticity: a shape close to a bell profile for the cyclones and the small anticyclones (with a lower amplitude for the cyclones) (Fig. 9C). For the large anticyclones, the vorticity followed the pattern described by Castelão and Johns (2011): a plateau in the core of the vortex, followed by a sharp transition to an annulus of cyclonic vorticity "shield" at the edge of the vortex (see their Fig. 6). In agreement with Castelão and Johns (2011), this shows that the large anticyclonic structures propagating along the western side of the Mozambique Channel are actually rings.

Table 1
Eddy properties derived from tracked eddies with a lifetime > 30 days, for number of eddies (N), mean lifetime ($\bar{\tau}$), mean amplitude ($\bar{\eta}$), and mean diameter ($\bar{L}$).

Eddy	N [eddies yr^{-1}]	$\bar{\tau}$ [day]	$\bar{\eta}$ [cm]	$\bar{L}$ [km]
Altimetry				
Cyclones	22.1	85.0	11.0	139.0
Anticyclones	17.1	101.0	14.0	157.0
SWIM				
Cyclones	17.5	53.0	9.0	137.0
Anticyclones	16.5	96.0	21.0	184.0
HYCOM				
Cyclones	29.7	76.0	6.0	106.0
Anticyclones	20.9	123.0	12.0	138.0

Fig. 10 presents the eddy mean characteristics (amplitude (n), total life-time (T) and travelling distance (D)) per class of radius (R by steps of 10 km) for AVISO, SWIM and HYCOM. In all datasets, for $R < 100$ km, the increase in n is associated with an increasing R. For AVISO (Fig. 10A) it followed a near-linear relationship ($y = 3.3 \times 10^{-6} \times R - 0.13$, $r = 0.77$). This relationship did not hold in the case of the rings (i.e. $R \geq 100$ km), with a mean amplitude of 28 cm. SWIM (Fig. 10B) and HYCOM (Fig. 10C) also reproduced a similar pattern to that observed in AVISO, although with a reduced slope. In SWIM the linear fit (for $R < 100$ km) is characterised by $y = 2 \times 10^{-6} \times R - 0.05$, ($r = 0.70$), and in HYCOM it is given by $y = 2.1 \times 10^{-6} \times R - 0.05$, ($r = 0.79$). SWIM overestimated the mean amplitude of the rings by 10 cm, while HYCOM only slightly overestimated by 2 cm.

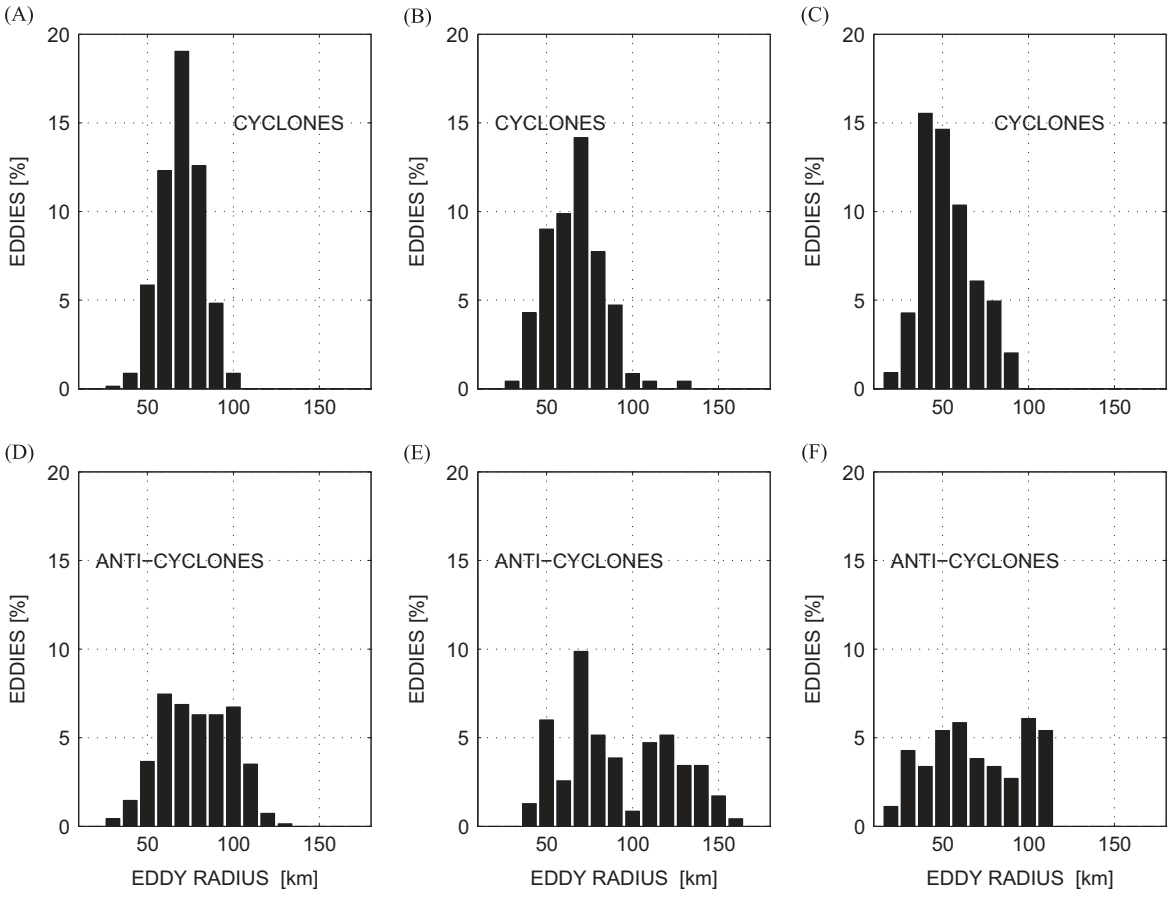

Fig. 8. Eddy density distribution as a function of the radius: (A, D) AVISO cyclones and anticyclones, (B, E) SWIM cyclones and anticyclones, (C, F) HYCOM cyclones and anticyclones.

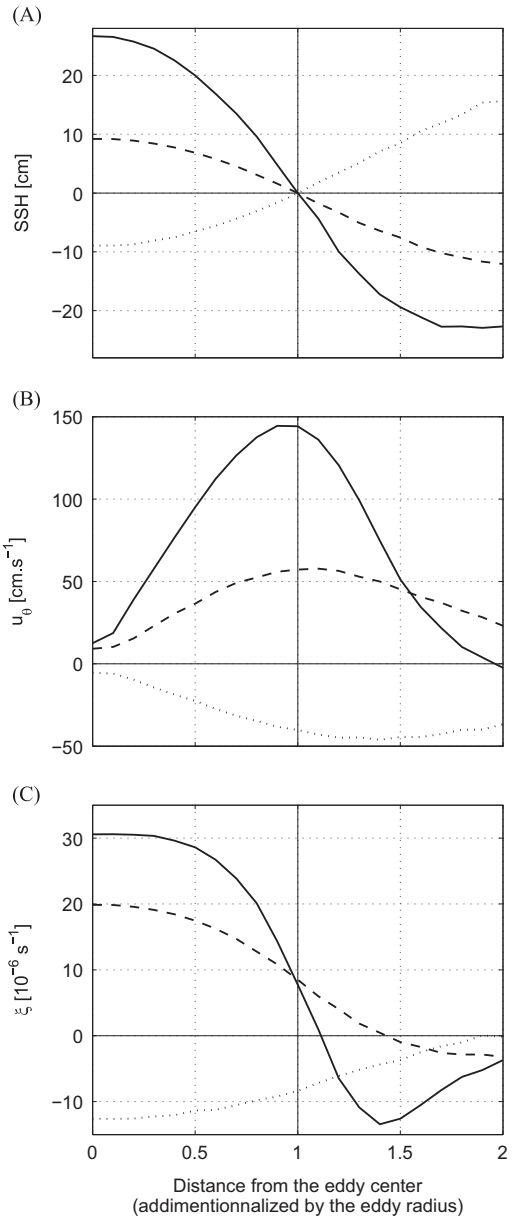

Fig. 9. (A) Mean eddy SSH, (B) azimuthal velocity, and (C) vertical Component Of vorticity, as a function of the distance from the centre, addimentionnalized by the eddy radius. Cyclones (dotted lines), anticyclones with a radius <100 km (dashed lines), anticyclones with a radius >100 km (plain lines).

Although there was a monotonous increase of the eddy lifetime with increasing radius, the eddy size distribution (for $R<100$ km) was statistically weak (Fig. 10D) when taking all the eddies with $R<100$ km into account. The rings in AVISO had a mean life expectancy of $\sim$127 days, while an average for SWIM was 12 days less, and in HYCOM 22 days longer.

There was no clear linear relationship for the eddy maximum travelling distance as a function of its radius. Although the models agreed in the representation of the travelling distance for the cyclonic structures that were below 500 km, they exaggerated the distance travelled by the rings, with a mean of 1463 km for SWIM and 1837 km for HYCOM (which is consistent with the longer life span of rings in HYCOM). For SWIM, the small anticyclones ($R<100$ km) had a longer life span (Fig. 10E) and travel further (Fig. 10H) than the cyclones. This pattern was not evident in HYCOM nor AVISO.

4. Discussion

By comparing the LOCO volume transport and its variability with the output from SWIM and HYCOM at 17°S, it was evident that the models were able to reproduce, with reasonable accuracy, the variability of the transport in the mesoscale range. Both models reproduced the mean transport although it was exaggerated in HYCOM. This could be associated with the representation of the remote influence of the Indonesian Throughflow in the basin-scale model used to provide the boundary conditions for the regional Agulhas HYCOM (George et al., 2010). The seasonal cycle was also exaggerated, particularly in SWIM. In this case, it may be related to the monthly climatological forcing fields used to drive the model. This was improved in HYCOM, that was forced using inter-annual fields and lateral boundary conditions.

At the mesoscale frequency range ($\sim$3 to 8 cycles yr^{-1}), the models were able to reproduce the observed power density spectra accurately (Fig. 3). The difference between the models and the observations was only $\sim$1 Sv^2 yr^{-1}. This suggested that, for these models, the misrepresentation of the eddy activity was not the cause of the exaggerated seasonal cycle. An alternative mechanism to that proposed by van der Werf et al. (2010) must therefore be responsible. A possibility could be associated with the variability of the wind field over the western Indian Ocean as proposed by Ridderinkhof et al. (2010).

At frequencies higher than the mesoscale (>8 cycles yr^{-1}), the power density spectra of SWIM and HYCOM were significantly less than observed. The underestimate in SWIM was almost two orders of magnitude, while in HYCOM it was approximately one order of magnitude. This underestimate of higher frequencies was most likely associated with small scale processes that were not resolved in the monthly climatology forcing in SWIM, and subgrid scale dynamics that the models were unable to resolve.

Both models were able to reproduce the pattern of SSH variability. It is important to mention that for both models and observation, the SSH variability was computed by removing the seasonal cycle. However, SWIM (Fig. 4B) appeared to exaggerate the level of variability in the centre of the Channel compared to observations, while in HYCOM (Fig. 4C) this was slightly under represented. For SWIM, the overestimation of the SSH variability appeared to be influenced by the observed overestimation of the mean amplitude and diameter of the anticyclonic eddies (Table 1), suggesting that the anticyclonic eddies dominated the signals of the mean SSH. On the other hand, for HYCOM, the under representation of the variability appeared to be influenced by the observed under estimation of the mean amplitude and diameter of the cyclonic eddies (Table 1). In terms of the spatial spreading of the SSH variability, SWIM appeared to overestimate the signals in the northern part of the channel, which seemed to originate at the northern tip of Madagascar and propagated into the Channel. In the southeast of the Channel (south of 20°S), both SWIM and HYCOM appeared to underestimate the spatial spread. This suggested that the models produced fewer eddies in this part of the channel.

The vertical structures of the eddies simulated by the two ocean models (Fig. 5) were in good agreement with observations (de Ruijter et al., 2002; Ridderinkhof and de Ruijter, 2003). Anticyclonic eddies observed at 17°S were wider, over 300 km, and had a strong barotropic signal, reaching the bottom, with velocities of 0.1 m s^{-1} (de Ruijter et al., 2002; Ridderinkhof and de Ruijter, 2003). This was also the case for the eddies simulated in SWIM and HYCOM (Fig. 5). The trajectories of the anticyclonic eddies on the western side of the Channel indicated that they were steered by topography. On the other hand, cyclonic eddies predominantly occurred at the edges of anticyclonic eddies, suggesting that cyclonic eddies may be spun up by the activity of anticyclonic eddies.

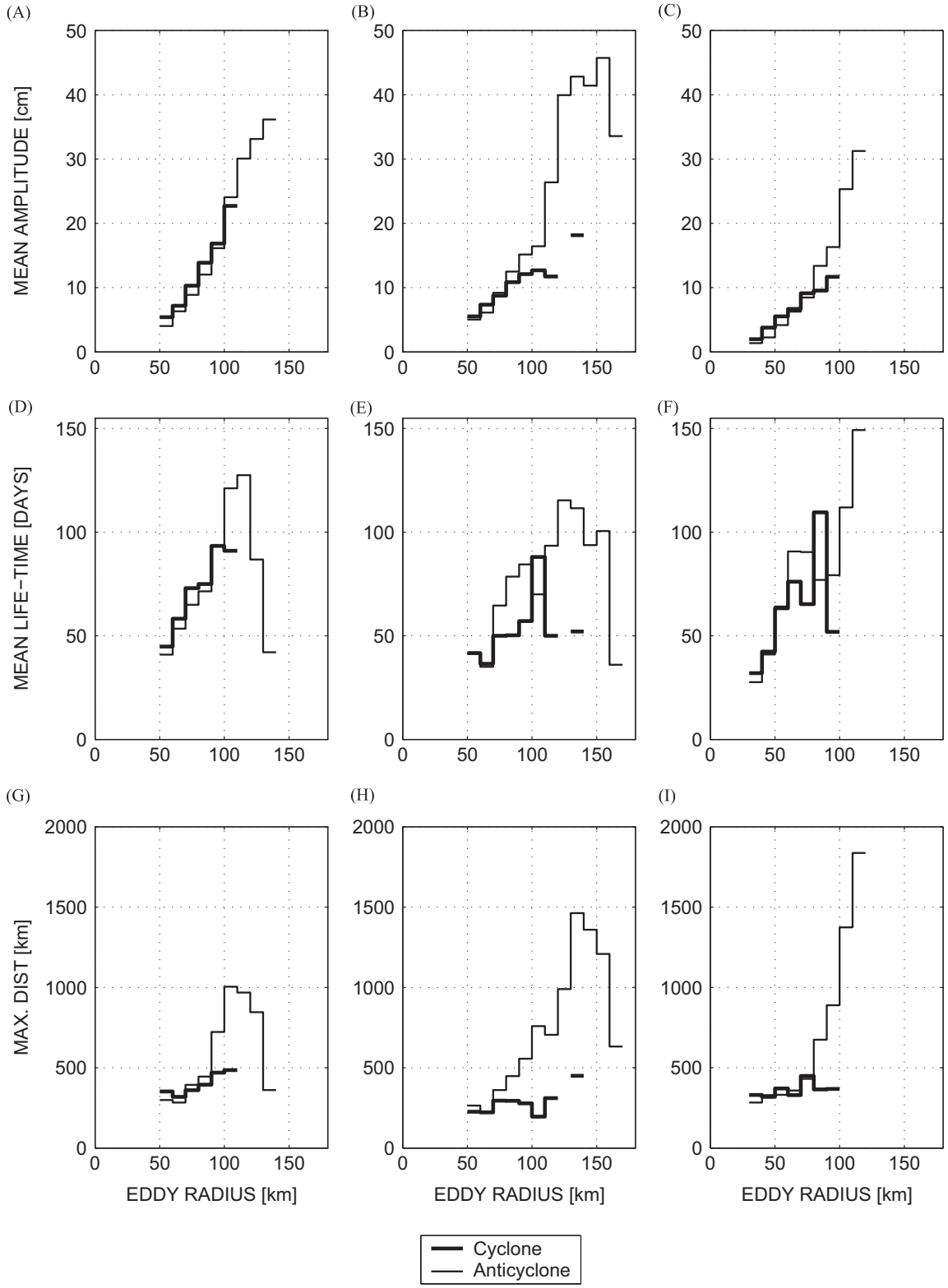

Fig. 10. (A–C) Eddy mean amplitude, (D–F) mean life-time, (G–I) maximum travelling distance, as a function of eddy radius, for AVISO (A,D,G), SWIM, (B,E,H) and HYCOM (C,F,I). Thick lines are cyclones; thin lines are anticyclones.

A preferential site for anticyclonic eddy formation appeared to be in the north around the Comoros Archipelago, at about 12°S between Madagascar and Mozambique. The centre of the Channel near 20°S, 43°E, also appeared to be a site favouring anticyclonic eddy formation. To the south of the tracking domain, anticyclonic eddy generation was also evident near 23°S, 43°E. This pattern was also evident in the ocean models, but less so in SWIM compared to HYCOM. This may be due to the higher resolution and longer time series of the HYCOM configuration.

The generation site identified around the Comoros Archipelago (Fig. 6) is in agreement with the eddy formation process discussed by Backeberg and Reason (2010). Positive vorticity (anticyclonic

vorticity) and shear instabilities are generated at Cape Amber by the friction between the SEC and the coastline (Biastoch and Krauss, 1999), contributing toward the eddy formation process. Although maximum shear occurs at Cape Amber, the eddies were only fully formed and detected to the west of the Cape. Note that to the west of Cape Amber lies the Comoros Archipelago, which consists of four islands extending zonally from Madagascar to the African continent, located in a region of rough topography characterised by shallow oceanic banks. These local features may also influence the generation of the eddies in the region.

Previous studies have shown that the generation of Mozambique Channel eddies may be related to the arrival of baroclinic Rossby waves that propagate westward across the Indian Ocean at 12°S (Schouten et al., 2002), or local generation of barotropic Rossby waves with periodicity of 50–55 days (Schott et al., 1988). Positive vorticity anomalies can be traced from Cape Amber to the western edge of the Mozambique Channel (Backeberg and Reason, 2010), where the eddies form (Fig. 6).

Cyclonic eddies have been shown to originate mostly along the eastern boundary of the Channel. Also, a localised site for generation of cyclonic eddies was evident at the western boundary of the Channel, near the narrows around ~16.5°S. This is consistent with the formation of lee coastal trapped cyclonic eddies mentioned by Lutjeharms (2006, see Fig. 3.25). Note that this is also a place where the Angoche upwelling occurs (Lutjeharms, 2006).

The cyclonic eddies generated in the eastern part of the central Channel propagated southwestward. The formation of cyclonic eddies within the Channel could explain the origin of some cyclonic eddies found in the work of Gründlingh (1995) and Quartly and Srokosz (2004). This also corroborates Harlander et al. (2009), who suggested that cyclonic eddies in this region could be expected, but weaker and less consistent when compared with the regular presence of the anticyclonic eddies.

The formation of cyclonic eddies near the southeastern boundary of the Channel was also enhanced. These eddies may be formed due to turbulence associated with currents interacting with the continental shelf of Madagascar. Furthermore, the tracking algorithm located a number of eddies formed to the southwest of Madagascar in all three data sets. This is in agreement with previous studies (Quartly and Srokosz, 2004; de Ruijter et al., 2004; Siedler et al., 2009), inferring that cyclonic eddies are generated by the friction at the inshore edge of the southern extension of the South East Madagascar Current with the continental shelf, as the current flows past the southern tip of Madagascar. Inspection of the region south of the tracking domain for AVISO provided evidence that some eddies could be generated outside of the Channel, especially southeast of Madagascar and migrate into the southern Mozambique Channel. This is consistent with previous observations by Quartly et al. (2006) and Morrow et al. (2004).

The large anticyclonic rings originating from the northern Mozambique Channel tended to propagate southwestwards following the African coastline (Fig. 7), in agreement with previous studies (Schouten et al., 2003). In contrast, anticyclonic eddies generated in the eastern part of the channel were smaller and their size was in a similar range to the single mode distribution of the cyclonic eddy field. This length scale is characteristic of baroclinic instabilities.

The frequency of occurrence of eddies (Fig. 7) closely agrees with the distribution of SSH variability (Fig. 4) and eddy trajectories (Fig. 6). The pattern confirmed the previous discussion regarding formation sites of eddies as well as their trajectories. AVISO and HYCOM suggested that the secondary anticyclonic eddy generation site (near 20°S, 43°E) was connected with the narrows of the Channel, whereas in SWIM such a connection was not evident, suggesting an independent eddy formation mechanism. More eddies have been found in HYCOM and less in SWIM, when compared to AVISO (Table 1). This was most likely associated with the higher horizontal resolution of the HYCOM configuration.

Cyclonic eddies were found to have a single mode distribution, associated with the Rossby radius of deformation. The anticyclonic eddies, on the other hand, appear to have a bi-modal distribution, suggesting two different formation mechanisms: mesoscale oceanic turbulence associated with the Rossby radius of deformation at that latitude, and a mechanism independent of the baroclinic Rossby radius of deformation, similar to Agulhas retroflection eddies, associated with the connection to South Equatorial Current.

In the first mode, SWIM simulated fewer eddies compared to AVISO, while in HYCOM there were more eddies. But in the second mode, SWIM and HYCOM simulated more rings than observed from altimetry, with more rings in SWIM than in HYCOM. Though the models appeared to produce a higher number of rings, they were in good agreement with observational studies reporting an average of 4–6 large anticyclones per year at the narrows of the Channel (de Ruijter et al., 2002; Schouten et al., 2003; Harlander et al., 2009; van der Werf et al., 2010). This result infers that the second mesoscale mode observed in our study was the passage of the rings which propagated parallel to the western boundary of the Channel, closely following the African coast (de Ruijter et al., 2002; Schouten et al., 2003; Harlander et al., 2009; van der Werf et al., 2010). It is likely that the first mesoscale mode (relatively smaller anticyclonic eddies) was related to the eddies generated to the south of the narrows of the Channel near the Madagascar coast. This may explain why the studies based on the LOCO moorings were not able to capture this mode.

The rings identified in this study (Fig. 9) have similar dynamical and geometrical structures to those observed in the North Brazil Current (NBC, Castelão and Johns (2011), see their Fig. 6). Goni and Johns (2001) using Topex/Poseidon altimeter data from 1992 to 1998 found an average formation rate of the NBC rings of about 1 per 2 months, suggesting a formation rate of 6 per year. Interestingly, this is close to 4–6 rings per year observed in this study. These NBC rings are deep, reaching ~2000 m (Wilson et al., 2002), and characterised by maximum SSH anomalies ranging between 5 to 30 cm, a radii of maximum velocity between 100 km and 160 km, and an overall size of about 400 km (Goni and Johns, 2001; Wilson et al., 2002; Castelão and Johns, 2011). These are relatively larger when compared with the rings found in this study and those observed by de Ruijter et al. (2002) and Schouten et al. (2003). While NBC rings are generated by the retroflection of the NBC (Fonseca et al., 2004), the rings found here appeared to be formed both by the shear of the SEC at the northern tip of Madagascar (Biastoch and Krauss, 1999), and also by the separation of the southward boundary flow from the northern Mozambique coast (Ridderinkhof and de Ruijter, 2003) at the northern entrance of the narrows of the Channel near 16°S (Fig. 6).

A consistent pattern was found between Fig. 9 and Fig. 10: the rings ($R \geq 100$ km) appear to exhibit different dynamical properties from the eddies ($R < 100$ km). The high correlation between the eddy mean amplitude with radius (Fig. 10) suggested that these eddies have a self-similar structure (Chelton et al., 2011) at regional scales, which holds a dependent variation. Such a uniform structure is broken with the superimposition of the rings (top panels, Fig. 10). The tendency of higher amplitudes in cyclonic eddies over the amplitude of the anticyclones observed for smaller scale eddies ($R < 80$ km, Fig. 10) can be explained by the theories of gradient wind effect of centrifugal force that works outwards in rotating eddies (Gill, 1982). This is described by Chelton et al. (2011) as intensifying the low pressure at the centre of the cyclones, while weakening the high pressure at the centre of the anticyclones.

Not surprisingly, as also reported by Chelton et al. (2011), it was observed that eddies with small amplitude or horizontal scale

have short life times, while large amplitude or horizontal scale eddies generally survive for longer periods (Fig. 10). This also appears to be the case for the maximum eddy travelling distance (Fig. 10). However, such a pattern was not observed in the case of the rings, corroborating the observation that the rings exhibit different dynamical properties from eddies Castelão and Johns (2011).

5. Summary

Satellite altimetry observations, transports from a mooring array and two different regional ocean models, were used to investigate eddy properties and transport variability in the Mozambique Channel. These models demonstrated a good agreement in the representation of transport variability at the mesoscale range, but overestimated the lower frequency signals (seasonal cycle), and underestimated the higher frequency signals. This could possibly be related to the forcing fields and boundary conditions (for overestimation), and also the subgrid-scale of unresolved processes in the models (for higher frequencies). The overestimation of the seasonal cycle in our case, was not related to a misrepresentation of the mesoscale variability.

Cyclonic and anticyclonic eddies, as well as rings, were found to be generated within the Channel. Cyclonic eddies appeared to be more abundant and smaller compared to anticyclonic eddies. Although cyclonic eddies seemed more ubiquitous than anticyclonic eddies, they were preferentially formed along the eastern part of the Channel. Anticyclonic eddies and rings appeared to be formed mostly in the northern sector near 12°S between Madagascar and the African continent. They propagated southward, parallel to the western boundary of the Channel, in agreement with previous studies. A new secondary site of anticyclonic eddy formation in the central eastern sector was also identified (near 20°S, 43°E).

Cyclonic structures had a single mode distribution, with a mean radius centred near the first baroclinic Rossby radius of deformation of the region. Anticyclonic structures, on the other hand, showed a bi-modal distribution, with the first mode also centred around a typical first baroclinic Rossby radius of deformation, and the second mode centred at larger scales around 100 km radius, suggesting that these are rings rather than eddies. The yearly average of these rings was consistent with previous observations of anticyclonic eddies propagating along the western boundary of the Channel. Eddy mean amplitude per class of radius (< 100 km) increased with increasing radius, while no linear relationship existed for the rings. The increase in the amplitude of the eddies was consistent with the increase in life expectancy and maximum travelling distances.

This study demonstrated that rigorous assessment of mesoscale variability in ocean models and comparing with available observations in a consistent manner, advances our quantitative understanding of mesoscale eddy dynamics, leading to new insights into eddy formation and propagation.

Acknowledgements

The principal author of this work gratefully acknowledges the IRD-DSF (France), the NRF and the Nansen-Tutu Centre for Marine Environmental Research (South Africa) for research funding. Data were obtained from the Netherlands Organization for Scientific Research (NWO) LOCO program, and from the French CNES and AVISO. We are also grateful to the reviewers for comments that helped us improve the paper.

References

Backeberg, B.C., Bertino, L., Johannessen, J.A., 2009. Evaluating two numerical advection schemes in HYCOM for eddy-resolving modelling of the Agulhas Current. Ocean Sci. 5, 173–190.
Backeberg, B.C., Johannessen., J.A., Bertino., L., Reason, C.J.C., 2008. The greater Agulhas Current system: an integrated study of its mesoscale variability. J. Oper.. Oceanogr. 1, 29–44.
Backeberg, B.C., Reason, C., 2010. A connection between the South Equatorial Current north of Madagascar and Mozambique Channel. Geophys. Res. Lett. 37, L04604.
Beal, L.M., Ruijter, W.P.M.D., Biastoch, A., Zahn, R., 2011. On the role of the Agulhas System in ocean circulation and climate. Nature 472, 429–436.
Biastoch, A., Böning, C.W., Lutjeharms, J.R.E., 2008a. Agulhas leakage dynamics affects decadal variability in Atlantic overturning circulation. Nature 456, 489–492.
Biastoch, A., Krauss, W., 1999. The role of mesoscale eddies in the source regions of the Agulhas Current. J. Phys. Oceanogr. 29, 2303–2317.
Biastoch, A., Lutjeharms, J.R.E., Böning, C.W., Scheinert, M., 2008b. Mesoscale perturbations control inter-ocean exchange South of Africa. Geophys. Res. Lett. 35, L20602.
Bleck, R., 2002. An oceanic general circulation model framed in hybrid isopycnic-cartesian coordinates. Ocean Model 37, 55–88.
Browing, G.L., Kreiss, H.O., 1982. Initialization of the shallow water equations with open boundaries by the bounded derivative method. Tellus 34, 334–351.
Browing, G.L., Kreiss, H.O., 1986. Scaling and computation of smooth atmospheric motions. Tellus 38, 295–313.
Castelão, G.P., Johns, W.E., 2011. Sea surface structure of North Brazil Current rings derived from shipboard and moored acoustic doppler current profiler observations. J. Geophys. Res. 116, CO1010.
Chaigneau, A., Gizolme, A., Grados, C., 2008. Mesoscale eddies off Peru in altimeter records: identification algorithms and eddy spatio-temporal patterns. Prog. Oceanogr. 79, 106–119.
Chassignet, E.P., Harley, H.E., Smedstad, O.M., George, R.H., Alan, J.W., Metzger, E.J., Brian, O.B., Carlos, L., Desiraju, B.R., Patrick, J.H., Ashwanth, S., 2006. Generalised Vertical Coordinates: for eddy-resolving global and coastal ocean forecasts. Oceanogr. Soc. 19, 118–129.
Chelton, D.B., deSzoeke, R.A., Schlax, M.G., Naggar, K.E., Siwertz, N., 1998. Geographical variability of the first-baroclinic rossby radius of deformation. J. Phys. Oceanogr. 28, 433–460.
Chelton, D.B., Schlax., M.G., Samelson, R.M., 2011. Global observations of nonlinear mesoscale eddies. Prog. Oceanogr. 91, 167–216.
Chelton, D.B., Schlax, M.G., Samelson, R.M., Szoeke, R.A., 2007. Global observations of large oceanic eddies. Geophys. Res. Lett. 34, L15606.
Conkright, M.E., Locarnini, R.A., Garcia, H.E., O'Brien, T.D., Boyer, T.P., Stephens, C., Antonov, J.I., 2002. World Ocean Atlas 2001: objective analyses, data statistics, and figures, CD-ROM documentation. Technical report, National Oceanographic Data Center, Silver Spring, MD.
Da Silva, A.M., Young, C.C., Levitus, S., 1994. Atlas of surface marine data 1994, vol. 1, algorithms and procedures. Technical report, U. S. Department of Commerce, NOAA.
Davies, H.C., 1983. Limitations of some common lateral boundary conditions used in regional NWP models. Mon. Weather. Rev. 111, 1002–1012.
de Ruijter, W.P.M., Biastoch, A., Drijfhout, S.S., Lutjeharms, J.R.E., Matano, R.P., Pichevin, T., van Leeuwen, P.J., Weijer, W., 1999. Indian-Atlantic interocean exchange: dynamics, estimation and impact. J. Geophys. Res. 104, 20885–20910.
deRuijter, W.P.M., Brummer, G.J.A., Drijfhout, S.S., Lutjeharms, J.R.E., Peeters, F., Ridderinkhof, H., vanAken, H., vanLeeuwen, P.J., 2006. Observations of the inter-ocean exchange around South Africa. Eos Trans. AGU 87, 97–101.
de Ruijter, W.P.M., Ridderinkhof, H., Lutjeharms, J.R.E., Schouten, M.W., Veth, C., 2002. Observations of the flow in the Mozambique Channel. Geophys. Res. Lett. 29, 1401–1403.
de Ruijter, W.P.M., van Aken, H.M., Beier, E.J., Lutjeharms, J.R.E., Matano, R.P., Schouten, M.W., 2004. Eddies and dipoles around South Madagascar: formation, pathways and large-scale impact. Deep Sea Res. Part I 51, 383–400.
Ducet, N., Le Traon, P.Y., Reverdin, G., 2000. Global high-resolution mapping of ocean circulation from TOPEX/Poseidon and ERS-1 and -2. J. Geophys. Res. 105, 19,477–19,498.
Fonseca, C.A., Goni., G.J., Johns, W.E., Campos, E.J.D., 2004. Investigation of the North Brazil Current retroflection and North Equatorial Countercurrent variability. Geophys. Res. Lett. 31, L21304.
George, M.S., Bertino., L., Johannessen., O.M., Samuelsen, A., 2010. Validation of a hybrid coordinate ocean model for the Indian Ocean. J. Oper. Oceanogr. 3, 25–38.
Gill, A.E., 1982. Atmosphere – Ocean Dynamics. Academic Press, New York.
Goni, G.J., Johns, W.E., 2001. A Census of North Brazil Current rings observed from Topex/Poseidon Altimetry: 1992–1998. Geophys. Res. Lett. 28, 1–4.
Gordon, A.L., 1986. Inter-ocean exchange of thermocline water. Geophys. Res. Lett. 91, 5037–5046.
Gründlingh, M.L., 1995. Tracking eddies in the southeast Atlantic and southwest Indian Oceans with TOPEX-POSEIDON. J. Geophys. Res 100, 24977–24986.
Haidvogel, D.B., Beckmann, A., 1999. Numerical ocean circulation modeling. Series on Environmental Science and Management, Vol. 2. Imperial College Press.
Halo, I., 2012. The Mozambique Channel eddies: characteristics and mechanisms of formation, (Ph.D. thesis). University of Cape Town.

Harlander, U., Ridderinkhof, H., Schouten, M.W., de Ruijter, W.P.M., 2009. Long-term observations of transport, eddies, and Rossby waves in the Mozambique Channel. J. Geophys. Res. 114, CO2003.
Isern-Fontanet, J., Garcia-Ladona., E., Font, J., 2006. Vortices of the Mediterranean Sea: an altimetric perspective. J. Phys. Oceanogr. 36, 87–103.
Kurian, J., Colas, F., Capet, X., McWilliams, J.C., Chelton, D.B., 2011. Eddy properties in the California Current System. J. Geophys. Res. 116, C08027.
Large, W.G., McWilliams, J.C., Doney, S.C., 1994. Oceanic vertical mixing: a review and a model with a nonlocal boundary layer parameterization. Rev. Geophys. 32, 363–403.
Lathuiliere, C., Levy, M., Echevin, V., 2011. Impact of eddy-driven vertical fluxes on phytoplankton abundance in the euphotic layer. J. Plankton. Res. 33, 827–831.
Legates, D., Willmott, C., 1990. Mean seasonal and spatial variability in gauge-corrected, global precipitation. J. Clim. 10, 111–127.
Lutjeharms, J.R.E., 2006. The Agulhas Current, Vol. 1. Springer-Verlag, Berlin.
Lutjeharms, J.R.E., van Ballegooyen, R.C., 1988. The retroflection of the Agulhas Current. J. Phys. Oceanogr. 18, 1570–1583.
Marchesiello, P., Debreu, L., Couvelard, X., 2009. Spurious diapycnal mixing in terrain-following coordinate models: the problem and a solution. Ocean Model. 26, 156–169.
Marchesiello, P., McWilliams, J.C., Shchepetkin, A., 2001. Open boundary condition for long-term integration of regional oceanic models. Ocean Model. 3, 1–21.
Morrow, R., Birol, F., Griffin, D., Sudre, J., 2004. Divergent pathways of cyclonic and anticyclonic eddies. Geophys. Res. Lett. 31, L24311.
Okubo, W., 1970. Horizontal dispersion of floatable particles in the vicinity of velocity singularities such as convergencies. Deep Sea Res. 17, 445–454.
Omta, A.W., Llido, J., Garcon, V., Kooijman, S.A.L.M., Dijkstra, H.A., 2009. The interpretation of satellite chlorophyll observations: the case of the Mozambique Channel. Deep Sea Res. I 56, 974–988.
Penven, P., Échevin, V., Pasapera, J., Colas, F., Tam, J., 2005. Average circulation, seasonal cycle and mesoscale dynamics of the Peru Current System: a modeling approach. J. Geophys. Res. 110, C10021.
Penven, P., Lutjeharms, J.R.E., Florenchie, P., 2006. Madagascar: a pacemaker for the Agulhas Current system? Geophys. Res. Lett. 33, L17609.
Penven, P., Marchesiello, P., Debreu, L., Lefèvre, J., 2008. Software tools for pre- and post-processing of oceanic regional simulations. Env. Model. Soft. 23, 660–662.
Quartly, G.D., Buck, J.J.H., Srokosz, M.A., Coward, A.C., 2006. Eddies around Madagascar - The Retroflection re-considered. J. Mar. Sys. 63, 115–129.
Quartly, G.D., Srokosz, M.A., 2004. Eddies in the southern Mozambique Channel. Deep Sea Res. II 51, 69–83.
Reason, C.J.C., Lutjeharms, J.R.E., Hermes, J., Biastoch, A., Roman, R., 2003. Inter-ocean exchange south of Africa in an eddy-permitting model. Deep Sea Res.II 50, 281–298.
Ridderinkhof, H., de Ruijter, W.P.M., 2003. Moored current observations in the Mozambique Channel. Deep Sea Res. II 50, 1933–1955.
Ridderinkhof, H., Lutjeharms, J.R.E., de Ruijter, W.P.M., 2001. A research cruise to investigate the Mozambique Current. S. Afr. J. Sci. 27, 461–464.
Ridderinkhof, H., van der Werf, P.M., Ullgren, J.E., van Aken, H.M., van Leeuwen, P.J., de Ruijter, W.P.M., 2010. Seasonal and interannual variability in the Mozambique Channel from moored current observations. J. Geophys. Res. 115, C06010.
Rio, M.H., Guinehut, S., Larnicol, G., 2011. The new CNES-CLS09 global mean dynamic topography computed from the combination of GRACE data, altimetry and in-situ measurements. J. Geophys. Res. 116, C07018.
Robinson, A.R., 1983. Eddies in Marine Science. Springer-Verlag, Berlin.
Schott, F.A., Fieux, M., Kindle, J., Swallow, J., Zantopp, R., 1988. The boundary currents east and north of Madagascar: 2 direct measurements and model comparisons. J. Geophys. Res. 93, 4963–4974.
Schouten, M.W., de Ruijter, W.P.M., van Leeuwen, P.J., 2002. Upstream control of Agulhas ring shedding. J. Geophys. Res. 107, C83109.
Schouten, M.W., de Ruijter, W.P.M., van Leeuwen, P.J., Ridderinkhof, H., 2003. Eddies and variability in the Mozambique Channel. Deep Sea Res. II 50, 1987–2003.
Shchepetkin, A.F., McWilliams, J.C., 2005. The regional oceanic modeling system (ROMS): a split-explicit, free-surface, topography-following-coordinate oceanic model. Ocean Model. 9, 347–404.
Siedler, G., Rouault, M., Biastoch, A., Backeberg, B., Reason, C.J.C., Lutjeharms, J.R.E., 2009. Modes of the southern extension of the East Madagascar Current. J. Geophys. Res. 114, C01005.
Slutz, G.L., Hiscox, S.L.J., Woodruff, S., Jenne, R., Joseph, D., Steurer, P., Elms, J., 1985. Inter-ocean exchange south of Africa in an eddy-permitting modelComprehensive ocean-atmosphere dataset; release 1, Climate Research Program. Technical report, NOAA Environmental Research Laboratories, Boulder, Colorado.
Song, Y., Haidvogel, D., 1994. A semi-implicit ocean circulation model using a generalised topography- following coordinate system. J. Comp. Phys. 115, 228–244.
Souza, J.M.A.C., de Boyer Montegut, C., Le Traon, P.Y., 2011. Comparison between three implementations of automatic identification algorithms for the qualification and characterization of mesoscale eddies in the South Atlantic Ocean. Ocean Sci. 7, 317–334.
Swart, N.C., Lutjeharms, J.R.E., Ridderinkhof, H., de Ruijter, W.P.M., 2010. Observed characteristics of Mozambique Channel eddies. J. Geophys. Res. 115, C09006.
Ternon, J-F., Bach, P., Barlow, R., Huggett, J., Jaquemet, S., Marsac, F., Menard, F., Penven, P., Potier, M., Roberts, M., 2013. The Mozambique Channel: from physics to upper trophic levels. Deep-Sea Res. II.
Tew-Kai, E., Marsac, F., 2009. Patterns of variability of sea surface chlorophyll in the Mozambique Channel: a quantitative approach. J. Mar. Sys 77, 77–88.
van der Werf, P.M., van Leeuwen, L.J., Ridderinkof, H., de Ruijter, W.P.M., 2010. Comparison between observations and models of the Mozambique Channel transport: seasonal cycle and eddy frequencies. J. Geophys. Res. 115, CO2002.
Weijer, W., de Ruijter, W.P.M., Dijkstra, H.A., van Leeuwen, P.J., 1999. Impact of Interbasin Exchange on the Atlantic Overturning Circulation. J. Phys. Oceanogr. 29, 2266–2284.
Weimerskirch, H., Le-Corre, M., Jaquemet, S., Potier, M., Marsac, F., 2004. Foraging strategy of a top predator in tropical waters: great frigatebirds in the Mozambique Channel. Mar. Ecol. Prog. Ser. 275, 297–308.
Weiss, J., 1991. The dynamics of enstrophy transfer in two-dimensional hydrodynamics. Physica D 48, 273–294.
Wilson, W.D., Johns, W.E., Garzoli, S.L., 2002. Velocity structure of North Brazil Current. Geophys. Res. Lett. 29, 1273.